

## Variation in the critical mass ratio of a freely oscillating cylinder as a function of Reynolds number

K. Ryan, M. C. Thompson, and K. Hourigan

*Fluids Laboratory for Aeronautical and Industrial Research (FLAIR), Department of Mechanical Engineering, Monash University, Clayton, Victoria 3800, Australia*

(Received 1 April 2004; accepted 8 October 2004; published online 8 February 2005)

A two-dimensional numerical investigation of the flow-induced vibration of a circular cylinder held free to oscillate transverse to the free-stream direction has been performed. The simulations were performed over a Reynolds number range  $Re=[30,200]$  and for an infinite reduced velocity. Two regions of high amplitude oscillations are observed and are referred to as the viscous and higher Reynolds number range, respectively. The viscous range was observed for  $Re=[40,95]$  and the higher Reynolds number range was observed above  $Re=180$ . A critical mass ratio, below which appreciable amplitude oscillations are observed, is determined as a function of Reynolds number. For Reynolds numbers between the two ranges, only very small oscillations were observed for all mass ratios investigated. © 2005 American Institute of Physics. [DOI: 10.1063/1.1850871]

The problem of flow-induced vibration of a rigid bluff body has generally been considered by studying an elastically mounted circular cylinder allowed to oscillate transverse to the fluid flow direction. Classical studies in the field have been restricted to consider only large mass ratio, highly damped cylinders; several comprehensive reviews exist on this topic (for example, Refs. 1–3).

Recent study of flow-induced vibration of a cylinder has extended the field to incorporate the effect of very low mass ratios and of very low structural damping forces.<sup>3–6</sup>

The study of Khalak and Williamson<sup>4</sup> demonstrated the existence of three oscillation “branches;” the initial, upper, and lower branch. Of interest is the upper branch, as it exhibits large amplitude oscillations. Khalak and Williamson<sup>4</sup> also demonstrated that the reduced velocity range over which significant amplitude oscillations were observed varied inversely with mass ratio. This work was extended by Govardhan and Williamson,<sup>5</sup> and a critical mass ratio was determined, below which large amplitude oscillations are maintained up to an infinite reduced velocity. They determined experimentally a critical mass ratio of  $m_{crit}^*=0.54$  for Reynolds numbers in the range  $Re=[2000,12\,000]$ . For cylinders with mass ratios below  $m_{crit}^*$ , they observed large amplitude oscillations up to the highest reduced velocity that could be achieved using their facilities.

By setting the structural restoring force  $k$  to zero, it is possible to study the case of an infinite reduced velocity, and this has been achieved both numerically and experimentally. In their experimental study, Govardhan and Williamson<sup>6</sup> observed high amplitude oscillations for  $m^* < 0.54$  for Reynolds numbers in the range  $Re=[4000,22\,000]$ . They also interpreted a critical mass ratio of 0.25 for  $Re=100$  from the results of the numerical study performed by Shiels *et al.*<sup>7</sup> In this study, we numerically determine the critical mass ratio for Reynolds numbers in the range  $Re=[30,200]$ .

The specific case considered here is that of a circular cylinder of density  $\rho$ , with diameter  $d$ , submerged in a homogeneous Newtonian fluid with density  $\rho_w$ , dynamic vis-

cosity  $\mu$ , and associated free stream velocity  $U_\infty$ . The cylinder is free to oscillate only in the direction transverse to the fluid flow. Two governing, nondimensional parameters describe the system completely, the Reynolds number,  $Re = \rho_w d U_\infty / \mu$ , and the cylinder mass ratio,  $m^* = \rho / \rho_w$ . In this study, the mass ratio is varied in the range  $m^* = [0.075, 0.8]$ .

Generally, for the case of flow-induced vibration, the reduced velocity  $U^* = U_\infty / f_n D$ , where  $f_n = \sqrt{k / (m + m_A)}$ ,  $k$  is the structural restoring force,  $m$  is the cylinder mass, and  $m_A$  is the added mass, is used as the governing flow field parameter, in preference to the Reynolds number. However, in this investigation, the structural restoring force is set to zero, and the reduced velocity is infinitely large for all Reynolds numbers and mass ratios considered. For this investigation, the structural damping force  $c$  was also set to zero, to ensure that the damping coefficient  $\zeta = c / 2\sqrt{k(m + m_A)}$  was always at the lower limiting case of  $\zeta = 0$ .

Therefore, for the system studied here, the governing equations of motion of the freely oscillating cylinder may be simply written in nondimensional form as

$$m^* \ddot{y}^* = C_L(t). \quad (1)$$

Here,  $\ddot{y}^* = \ddot{y} \pi D / 2 U_\infty^2$  is the normalized cylinder acceleration and  $C_L$  is the lift force coefficient.

The flow field is determined by solving the two-dimensional form of the incompressible Navier–Stokes equations. A Galerkin spectral-element method is used to discretize the spatial domain; this is coupled with a three-step time splitting algorithm to advance the solution forward in time. The algorithm solves the equations governing the fluid-structure interaction in a noninertial reference frame, held fixed relative to the cylinder. The forces acting on the cylinder are calculated by determining the viscous and pressure components directly from the flow field solution. The Navier–Stokes equations are coupled to the equations of motion through the lift force and the cylinder position is updated at each time step using a predictor-corrector technique.

Details of the predictor-corrector technique have already been described fully.<sup>8</sup> A full description of the flow-field solution technique is beyond the scope of this paper, however, details may be found in Thompson *et al.*<sup>9</sup> and references therein.

The domain chosen for the investigation consists of 518 macroelements, an inlet boundary condition 15 diameters upstream of the cylinder, and an outlet (Neumann) boundary condition 23 diameters downstream of the cylinder; the wall boundaries on either side of the cylinder are 15 diameters away from the cylinder and have an inlet condition imposed. A rigorous domain study has been performed for the case of both a stationary and freely oscillating cylinder,<sup>8</sup> revealing a blockage effect of less than 2% for  $Re=200$ . A rigorous mesh independence study was also performed. From the results of this study, eighth order polynomial interpolants were used to discretize the domain within each macroelement. The current numerical scheme has been validated by comparing results with those of Blackburn and Henderson<sup>10</sup> at  $Re=250$ ; the current code reproduced their predictions to within numerical error. A full description of the code validation is presented by Ryan.<sup>8</sup>

For each Reynolds number and cylinder mass ratio, the simulation is performed until a saturated solution is obtained. The cylinder position is obtained as a function of time, and from this information an amplitude of oscillation is calculated. Following Govardhan and Williamson,<sup>6</sup> the oscillation results are shown in the  $(A^*, f^*)$  plane where  $f^* = f_{v0}/f$ ,  $f_{v0}$  is the Strouhal shedding frequency from a fixed cylinder and  $f$  is the oscillation frequency, and  $A^* = A/D$  is the normalized amplitude of oscillation taken as half the normalized peak-to-peak value. By presenting the results in this plane, amplitude information and lock-in information can both be clearly indicated (here lock-in describes a system where  $f^* \neq 1$  and the oscillations of the cylinder are synchronized with the shedding frequency). Results are also presented in the  $(f^*, m^*)$  plane, which clearly shows the effect of a changed mass ratio on the frequency response of the system.

Figure 1 shows the results for Reynolds numbers in the range  $Re=[40,100]$ . Simulations were also performed at  $Re=30$ , however, cylinder oscillations were not observed at this low Reynolds number. This is in agreement with the findings of Taneda,<sup>11</sup> who, in his study of the flow past a fixed cylinder, did not observe global instabilities for Reynolds numbers below  $Re=35$ .

For  $Re=40$ , the response was markedly different for all mass ratios when compared to simulations performed at slightly higher Reynolds numbers ( $Re=[50,70]$ ); the largest amplitude observed being  $A_{max}^* \approx 0.14$  for  $m^*=0.2$  (the lowest mass ratio considered for  $Re=40$ ); also,  $f^*$  decreased below  $f^*=1$  for all mass ratios considered, this is in contrast to all higher Reynolds numbers considered. Further,  $A^*$  approaches zero as  $m^*$  is increased for  $Re=40$ . By contrast, for higher Reynolds numbers  $A^*$  approaches a finite value as  $m^*$  approaches the maximum value investigated.

For Reynolds numbers in the range  $Re=[50,90]$ ,  $f^* > 1$  for all simulations conducted, indicating that the shedding cycle was locked-in with the oscillating frequency for all mass ratios considered. For each Reynolds number, for small

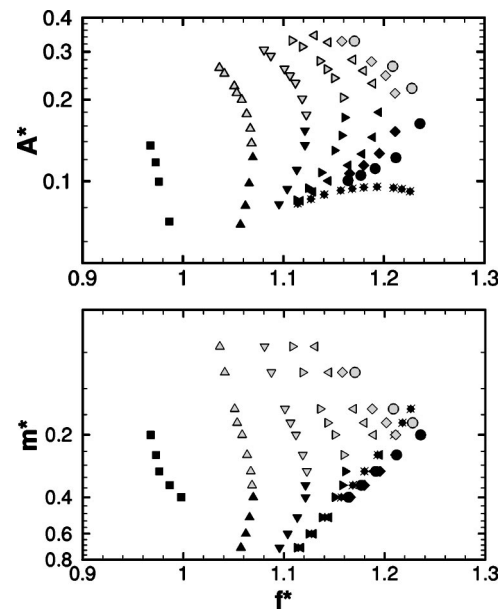


FIG. 1. Amplitude of oscillation and mass ratio response as a function of frequency ratio for Reynolds numbers in the range  $Re=[40,100]$ ; ■,  $Re=40$ ; ▲,  $Re=50$ ; ▼,  $Re=60$ ; ►,  $Re=70$ ; ◄,  $Re=80$ ; ◆,  $Re=85$ ; ●,  $Re=90$ ; and \*,  $Re=100$ . Hollow points indicate values where  $A^* > A_{critical}^*$ .

amplitude oscillations,  $f^*$  increases with  $A^*$ . For a critical value of  $A^*$  (hereafter referred to as  $A_{critical}^*$ ), a maximum value of  $f^*$  is reached. For oscillation amplitudes higher than this critical value,  $f^*$  decreases with increasing  $A^*$ . Within the Reynolds number range shown in Fig. 1, increasing the Reynolds number acts to increase both the range and variation of  $f^*$  as a function of  $A^*$ . Also apparent is that as the Reynolds number is increased, fewer simulations found  $A^* > A_{critical}^*$ , from Fig. 1, this corresponds to the mass ratio at which  $A_{critical}^*$  occurs decreasing with increasing Reynolds number in this range. Despite the significant difference in Reynolds numbers when comparing investigations, the current results are in qualitative agreement with those found experimentally by Govardhan and Williamson.<sup>6</sup> They found, for  $A^* < A_{critical}^*$ , the oscillation response was quasiperiodic. By contrast, at these low Reynolds numbers no quasiperiodic state was observed.

As the Reynolds number is increased further to  $Re=100$ , a value of  $A_{critical}^*$  [i.e., a turning point in the  $(A^*, f^*)$  response] is not observed for any mass ratio considered. Indeed, the amplitude of oscillation is observed to decrease with decreasing mass ratio. This result is contrary to the findings at all Reynolds numbers less than 100.

Figure 2 shows the cylinder oscillation response as the Reynolds number is increased through the range  $Re=[100,200]$ . This figure clearly shows that the findings for  $Re=100$  presented in the previous figure are not restricted to only the  $Re=100$  case. For Reynolds numbers in the range  $Re=[100,170]$  only small amplitude oscillations were observed ( $A^* \approx 0.1$ ) even for the lowest mass ratio considered ( $m^*=0.075$ ), indeed, within this Reynolds number range, the amplitude actually decreases slightly with decreasing mass ratio. As with simulations performed at lower Reynolds numbers, the oscillations observed for  $Re=[100,200]$  were syn-

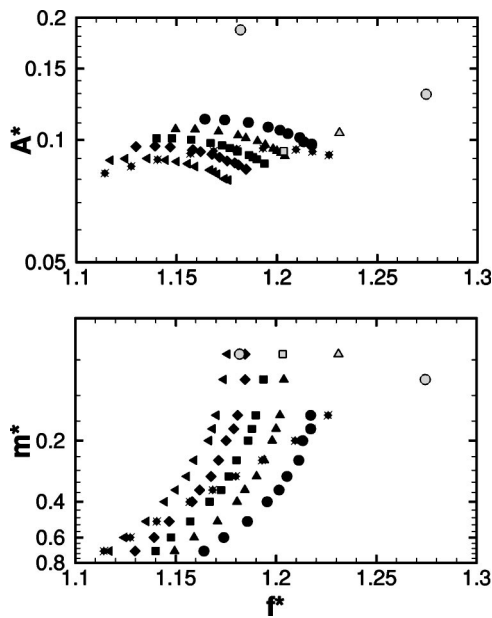


FIG. 2. Amplitude of oscillation and mass ratio response as a function of frequency ratio for Reynolds numbers in the range  $Re=[100,200]$ ; \*,  $Re=100$ ; ◀,  $Re=150$ ; ◆,  $Re=170$ ; ■,  $Re=180$ ; ▲,  $Re=190$ ; and ●,  $Re=200$ . Hollow points indicate values where  $A^* > A^*_{critical}$ .

chronized with the shedding frequency for all mass ratios considered.

As the Reynolds number is increased to  $Re=180$ , a barely perceptible, abrupt increase in the amplitude is noted as the mass ratio is reduced from  $m^*=0.1$  to  $m^*=0.075$ . This increase is more evident as the Reynolds number is increased to 190. As the Reynolds number is further increased to 200, a marked increase in amplitude is observed for mass ratios below  $m^*=0.15$ . This increase in amplitude is associated with an increase in  $f^*$ . For  $Re=200$  an  $A^*_{critical}$  value appears, coinciding with  $m^*=0.1$ ; for  $m^*=0.075$ ,  $f^*$  decreases. Of note is that for  $Re=200$  the oscillations exhibited for  $A^* \approx A^*_{critical}$  ( $m^*=0.1$ ) are quasiperiodic, in agreement with previous findings.<sup>6</sup>

From the response characteristics presented in Figs. 1 and 2 it is evident that two response ranges exist, which vary as a function of Reynolds number. The first range ( $Re=[40,95]$ ) is tentatively referred to as the “viscous” range. For these low Reynolds numbers, the viscous component contributes a significant proportion to the total force acting on a stationary cylinder.<sup>12</sup> The second Reynolds number range is referred to as the “higher” Reynolds number range, beginning at  $Re \approx 180$ . The higher Reynolds number range continues up to the highest Reynolds number considered in this study and may continue up to even higher Reynolds numbers.

Figure 3 shows the maximum peak amplitude response obtained for each Reynolds number investigated. This figure clearly shows the two response ranges as regions where  $A^*_{max}$  is significant. Also shown for comparison is the response of Shiels *et al.*<sup>7</sup> for  $Re=100$  and  $m^*=0.16$ ; this amplitude response was the highest they obtained for a finite  $m^*$  and compares favorably with the present results.

In both the viscous and higher Reynolds number range,

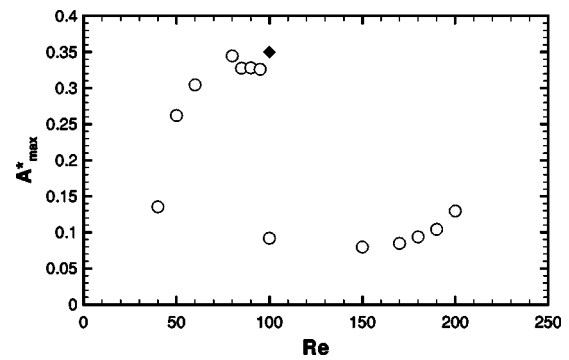


FIG. 3. (○) Maximum oscillation amplitude as a function of Reynolds number for cylinder mass ratios in the range  $m^*=[0.075,0.7]$  and  $Re=[40,200]$ . (◆) Oscillation amplitude results for Shiels *et al.* (Ref. 7) with  $m^*=0.16$ ,  $k=0$ ,  $c=0$ , representing the highest oscillation amplitude reported for a finite  $m^*$ .

$A^*_{max}$  coincides with the amplitude of oscillation for  $m^*=0.075$ , the lowest mass ratio considered. Given the form of the relationship between  $A^*$  and  $m^*$  (which may be inferred from Figs. 1 and 2), it is probable that  $A^*_{max}$  is slightly greater for the limiting case of  $m^*=0$  than that presented in Fig. 3.

It should also be noted that for a given Reynolds number,  $A^*_{max}$  reported here is lower than that reported previously for studies performed within the present Reynolds number range investigated.<sup>7,13,14</sup> With the exception of the work by Shiels *et al.*,<sup>7</sup> the value of  $A^*_{max}$  reported previously was for a finite reduced velocity. Experimental work,<sup>5,6</sup> performed at much higher Reynolds numbers, has shown that, for  $m^* < m^*_{crit}$ , the amplitude of oscillation decreases somewhat at an infinite reduced velocity when compared to a finite reduced velocity, but the amplitude is still significantly large. The numerical study by Shiels *et al.*<sup>7</sup> at  $Re=100$  shows the same trend. For finite mass ratios, their highest amplitude recorded was  $A^*=0.58$  at  $U^*=0.71$  and  $m^*=2.5$ ; by contrast, for  $U^*=\infty$ , they found the highest amplitude of oscillation to be  $A^*=0.35$  for  $m^*=0.25$ , as shown in Fig. 3.

Following the definition used in prior studies,<sup>6</sup> a critical mass ratio was calculated for each of the Reynolds numbers investigated. Here, the critical mass ratio is defined as the highest mass ratio which exhibits synchronized oscillations and for which  $A^* \geq A^*_{critical}$ . This corresponds to the mass ratio at which a jump in the amplitude response is observed. This definition allows for the variation in peak amplitude response as a function of Reynolds number. It also allows for a critical mass ratio to be defined even where  $A^*$  appears to increase smoothly with decreasing  $m^*$ . This definition coincides with the definition used previously<sup>5</sup> that  $m^*_{crit}$  corresponds to the mass ratio below which significant amplitude oscillations are observed up to and including  $U^*_{\infty}$ .

Figure 4 shows the calculated value of  $m^*_{crit}$  as a function of Reynolds number. Note that a critical mass ratio is not defined in the range  $Re=[100,170]$ , as no jump in  $A^*$  was observed below any specific mass ratio for all values considered. It is possible that in this Reynolds number range, a critical mass ratio less than  $m^*_{crit}=0.075$  exists. Also shown is the value of  $m^*_{crit}$  determined by Govardhan and Williamson<sup>6</sup> of  $m^*_{crit}=0.25$  for  $Re=100$  (determined from the numerical

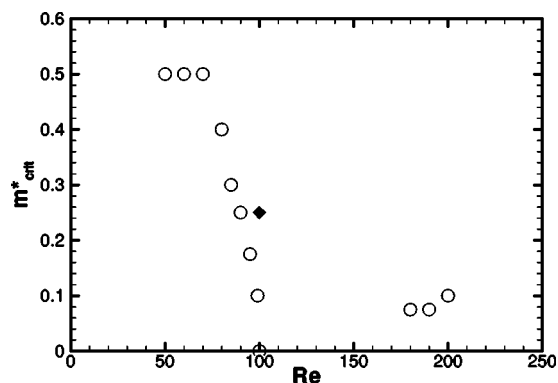


FIG. 4. Variation in the critical mass ratio as a function of Reynolds number;  $\circ$ , present results;  $\blacklozenge$ , Govardhan and Williamson's (Ref. 6) estimate of the simulations of Shiels *et al.* (Ref. 7).

results of Shiels *et al.*<sup>7</sup>). The present results compare favorably with this finding.

The present results have shown evidence for two regions of critical mass ratio, a low Reynolds number, viscous region, and a higher Reynolds region. Between these two regions (in the range  $Re \approx [100, 170]$ ) no critical mass ratio was found. These results should not be taken to suggest that high amplitude oscillations are impossible in the range  $Re \approx [100, 170]$ ; just that, if high amplitude oscillations are possible, they will only be observed up to a finite reduced velocity.

Three-dimensional direct numerical simulation studies at higher Reynolds numbers (specifically in the range  $Re = [300, 2000]$ ) will be able to account for three-dimensional effects on the critical mass ratio. This work is continuing.

The first author would like to acknowledge support provided through a Monash Departmental Scholarship. The au-

thors would like to acknowledge strong support from the Victorian Partnership for Advanced Computing and the Australian Partnership for Advanced Computing which enabled this research to take place.

- <sup>1</sup>T. Sarpkaya, "Vortex-induced oscillations," *J. Appl. Phys.* **46**, 241 (1979).
- <sup>2</sup>B. M. Sumer and J. Fredsoe, *Hydrodynamics around Cylindrical Structures* (World Scientific, Singapore, 1997).
- <sup>3</sup>C. Williamson and R. Govardhan, "Vortex-induced vibrations," *Annu. Rev. Fluid Mech.* **36**, 413 (2004).
- <sup>4</sup>A. Khalak and C. Williamson, "Motions, forces and mode transitions in vortex-induced vibrations at low mass-damping," *J. Fluids Struct.* **13**, 813 (1999).
- <sup>5</sup>R. N. Govardhan and C. H. K. Williamson, "Modes of vortex formation and frequency response of a freely vibrating cylinder," *J. Fluid Mech.* **420**, 85 (2000).
- <sup>6</sup>R. N. Govardhan and C. H. K. Williamson, "Resonance forever: existence of a critical mass and an infinite regime of resonance in vortex-induced vibration," *J. Fluid Mech.* **473**, 147 (2003).
- <sup>7</sup>D. Shiels, A. Leonard, and A. Roshko, "Flow-induced vibration of a circular cylinder at limiting structural parameters," *J. Fluids Struct.* **15**, 3 (2001).
- <sup>8</sup>K. Ryan, "The analysis of wake structures behind stationary, freely oscillating and tethered cylinders," Ph.D. thesis, Department of Mechanical Engineering, Monash University, Victoria, Australia, 2004.
- <sup>9</sup>M. C. Thompson, K. Hourigan, and J. Sheridan, "Three-dimensional instabilities in the wake of a circular cylinder," *Exp. Therm. Fluid Sci.* **12**, 190 (1996).
- <sup>10</sup>H. M. Blackburn and R. D. Henderson, "Lock-in behavior in simulated vortex-induced vibration," *Exp. Therm. Fluid Sci.* **12**, 184 (1996).
- <sup>11</sup>S. Taneda, "Experimental investigation of the wakes behind cylinders and plates at low Reynolds numbers," *J. Phys. Soc. Jpn.* **11**, 302 (1956).
- <sup>12</sup>R. Henderson, "Details of the drag curve near the onset of vortex shedding," *Phys. Fluids* **7**, 2102 (1995).
- <sup>13</sup>D. Newman and G. E. Karniadakis, "Simulations of flow over a flexible cable. comparison of forced and flow-induced vibration," *J. Fluids Struct.* **10**, 439 (1996).
- <sup>14</sup>H. M. Blackburn and G. Karniadakis, "Two- and three-dimensional simulations of vortex-induced vibration of a circular cylinder," Proceedings of the Third International Offshore and Polar Engineering Conference, Singapore, 6–11 June 1993.